



# Structural and Electrical Properties of Lead-Free Perovskite: $\text{Bi}(\text{Sr}_{0.25}\text{Ti}_{0.25}\text{Fe}_{0.5})\text{O}_3$

Varsa Purohit<sup>1</sup> · R. N. P. Choudhary<sup>1</sup> · Madhusmita Sahu<sup>1</sup>

Received: 30 December 2019 / Accepted: 27 January 2020 / Published online: 3 February 2020  
© Springer Science+Business Media, LLC, part of Springer Nature 2020

## Abstract

The polycrystalline bismuth strontium ferric titanate ( $\text{Bi}(\text{Sr}_{0.25}\text{Ti}_{0.25}\text{Fe}_{0.5})\text{O}_3$ ), synthesized via a high-temperature solid-state reaction route, has been characterized by using different experimental procedures. Study of basic crystal structure with the help of X-ray diffraction data of the compound exhibits the rhombohedral crystal system. The quality of the sample was asserted by studying its microstructure and morphology. Detailed investigations of dielectric and electrical properties of  $\text{Bi}(\text{Sr}_{0.25}\text{Ti}_{0.25}\text{Fe}_{0.5})\text{O}_3$  in a broad frequency (1 kHz–1 MHz) and temperature (25–450 °C) ranges have provided various important information on conduction mechanism, structure-properties relationship, etc. The high dielectric constant and relatively low tangent loss with multiple phase transitions have been observed in the material in the experimental frequency and temperature ranges.

**Keywords** Lead free ceramic · Rhombohedral structure · Non Debye relaxation

## 1 Introduction

The design and development of electronic materials for device applications are generally based on structural type and their properties. The majority of the functional materials developed so far for variety of applications are oxides of different structural families, such as perovskite, tungsten bronze, layer structure, etc. Among them, a large number of materials belong to perovskite structural family because of their interesting physical and chemical properties with structural stability required for device applications. Perovskite usually represents a type of crystal structure of a general formula  $\text{ABX}_3$ , in which A and B are cations and X is anion. In a cubic perovskite structure, A cation sits at the corner position, B cation sits at body centered position and anion sits at face centered position [1, 2]. In an ideal cubic structure, the A cation has a 12-fold cubooctahedral coordination, whereas the B cation has sixfold coordination surrounded by an octahedrons of anions. In 1839, Gutsove rose discovered the first perovskite  $\text{CaTiO}_3$  in the Ural Mountains of Russia

[3]. The structure “Perovskite” has been named after Russian mineralogist Lev Perovski. Later many inorganic metal oxides, like  $\text{PbTiO}_3$ ,  $\text{BaTiO}_3$ ,  $\text{SrTiO}_3$ ,  $\text{BiFeO}_3$  were found to have the perovskite structure. These oxides are used in a variety of industrial applications due to their ferroelectric, piezoelectric, dielectric, etc. Properties out of many perovskite oxides, some compounds, like  $\text{LiNbO}_3$ ,  $\text{BiFeO}_3$ ,  $\text{PbTiO}_3$  show photo Voltaic (PV) effect due to their ferroelectric polarization and other properties. As they do not show good semiconducting properties, they are suitable for PV applications [4, 5].

Recently, a major attention has been given towards developing dielectric ceramics having high dielectric constant and low tangent loss for designing devices in electronic system, which can be operated at high temperature [6, 7]. Some lead-based ferroelectric ceramics are mainly used in piezoelectric appliances. Lead titanate ( $\text{PbTiO}_3$ )-based perovskite compounds including  $\text{Pb}(\text{ZrTi})\text{O}_3$  with an morphotropic phase boundary (MPB) build up a majority of the actual market of piezoelectric materials [8]. But recent concerns on using lead-free materials for devices is more noticeable because of the toxic nature of lead based materials which should be avoided. They can cause severe harmful and harsh effect to the environment and human life. In view of the above, bismuth-constituent oxide systems are considered to be a suitable substitute to lead-based materials [9, 10]. On account

✉ Varsa Purohit  
varsapurohit94@gmail.com

<sup>1</sup> Department of Physics, Siksha ‘O’ Anusandhan (Deemed To Be University), Khandagiri, Bhubaneswar, Odisha 751030, India

of specific aspect of the electronic configuration of  $\text{Bi}^{3+}$  cation similar to the  $\text{Pb}^{2+}$  cation–shell structure, bismuth-containing compounds show generally ferroelectricity and relative behaviour. In addition, due to small cationic size, the oxygen-octahedral compounds with  $\text{Bi}^{3+}$  ions in positions having a coordination number higher than 6 crystallize mainly in pyrochlore or layered perovskite-like structures [11]. Moreover, the oxide compounds of a general chemical formula,  $\text{ABO}_3$  (A = mono-divalent, B = tri- to penta-valent ions) crystallize in the above mentioned perovskite and perovskite related structure [12]. Such type of compounds have recently attracted much attention because of the interesting physics behind its structure and properties and its potential application.  $\text{BiFeO}_3$  is a rhombohedrally distorted perovskite structure with R3c space group. It becomes most important for applications because of its high ferroelectric and antiferromagnetic phase transitions (ferroelectric transition temperature  $T_c = 830$  °C, magnetic transition temperature  $T_N = 370$  °C) [13]. The magnetic moment of iron of the B-site is ferromagnetically coupled with in the (1 1 1) plane, and antiferromagnetically coupled between the adjacent planes showing G- type antiferromagnetism. The macroscopic magnetization can be resulted, when the magnetic moment is oriented perpendicular to the (1 1 1) direction, and thus symmetry allows a canting ferromagnetic sublattice. However, superimposed on the antiferromagnetic ordering, there is a spiral spin structure in which the antiferromagnetic axis rotates through the crystal with an incommensurate long-wavelength period of 620 Å. It can be suppressed by doping and inhibits the linear magnetoelectric effect (weak ferromagnetism and magnetoelectric coupling in bismuth ferrite). Though bismuth ferrite with its multiferroic properties is useful for high temperature multifunctional applications, it suffers with some serious inherent problems, such as high leakage current, structural instability and distortion, existence of impurity phase, etc. Therefore, there have been constant efforts to resolve the problems and improve the dielectric properties by modifying Bi or/and Fe-site with suitable substituents and formation of solid solution/composites with similar or different structures [14–22]. In order to get single-phase bismuth ferrite to enhance multifunctionality, many synthesis routes have been attempted, for instance, liquid phase sintering method, sol–gel method, thin film, etc. [23, 24]. Doping or substitution is a main and convenient approach to enhance the electrical properties of the material prepared by different methods including a solid-state method. In the present study, an attempt has been made to modify bismuth ferrite with similar perovskite compound  $\text{SrTiO}_3$  or Sr/Ti to get new chemical composition of bismuth ferrite (i.e.,  $\text{Bi}(\text{Sr}_{0.25}\text{Ti}_{0.25}\text{Fe}_{0.5})\text{O}_3$  (BSTF)). Detailed literature survey on this compound suggests that not much work on structural and electrical (dielectric, impedance, conductivity, etc.) properties of  $\text{Bi}(\text{Sr}_{0.25}\text{Ti}_{0.25}\text{Fe}_{0.5})\text{O}_3$  (BSTF),

has been reported until now. In consideration of the significance of this lead-free compound, we have synthesized and methodically carried out structural and electrical characterization of the compound, which is reported here.

## 2 Experimental Details

The polycrystalline  $\text{Bi}(\text{Sr}_{0.25}\text{Ti}_{0.25}\text{Fe}_{0.5})\text{O}_3$  (BSTF) was prepared by a solid state reaction route using high-purity compounds;  $\text{Bi}_2\text{O}_3$  (M/S CDH),  $\text{Sr}_2\text{CO}_3$  (M/S Loba Chemie Co., Ltd.),  $\text{TiO}_2$  (M/S Loba Chemie Co., Ltd.) and  $\text{Fe}_2\text{O}_3$  (M/S Loba Chemie Co., Ltd.). All the powders were weighed stoichiometrically and ground in dry and wet medium for 3 h each to get a homogeneous mixture. After that the mixture was placed in a crucible in a muffle furnace at 900 °C for 4 hours for calcinations. Then the lumped formed during calcination was crushed and ground to make fine and smooth powder of the compound. The X-ray diffraction (XRD) experiment was performed at room temperature with the help of Bruker D8 diffractometer to study the structure of BSTF. After confirming the structure of the compound, a small amount of polyvinyl alcohol (organic binder) was mixed to the powder to make the pellets, which can be evaporated at higher temperature during the time of sintering. The cylindrical pellets of diameter 1.2 cm and thickness 0.1–0.2 cm were fabricated at a pressure of  $4 \times 10^7$  N/m<sup>2</sup> using KBR hydraulic press, and sintered them in the furnace at 900 °C for 4 h. A silver paint was applied on the both sides of a pellet (working as electrode) sample following with heating at 150 °C for an hour, in order to the measurement of impedance and dielectric parameters. The dielectric, impedance, conductivity, and modulus data were acquired using a computer-connected LCR (phase sensitive meter—PSM 1735, N4L) in a wide frequency range (1 kHz to 1 MHz) at various temperatures (25–500 °C).

## 3 Results and Discussion

### 3.1 Structure and Microstructure

To identify the phase formation with unit cell parameters of newly made perovskite  $\text{Bi}(\text{Sr}_{0.25}\text{Ti}_{0.25}\text{Fe}_{0.5})\text{O}_3$ , XRD (Fig. 1a) data were collected in a broad range of Bragg angle with the help of Cu- target (wave length = 1.5418 Å) using X-ray powder diffractometer. The observed peaks of the pattern were indexed using the Bragg angle of diffraction peaks in the different crystal structure and three unit cell configurations by means of a software named as ‘POWD’ [25] to find the structural data of an unidentified system. On the basis of the finest fitting of some basic structural data or parameters (minimum difference

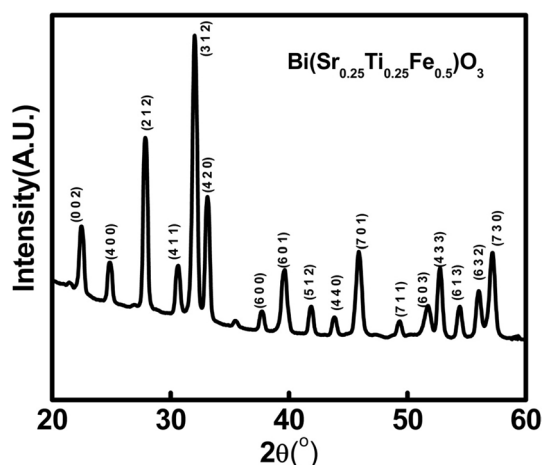


Fig. 1 XRD pattern of  $\text{Bi}(\text{Sr}_{0.25}\text{Ti}_{0.25}\text{Fe}_{0.5})\text{O}_3$

between theoretical and experimental value of inter-planar distance or Bragg angle of individual reflection), a fit crystal structure and unit cell dimensions for the sample BSTF were selected. It can be found from the data (diffraction) that the BSTF can have rhombohedral structure. The least-squares unit cell dimensions are:  $a = 16.5283 \text{ \AA}$ ,  $c = 7.9103 \text{ \AA}$ ,  $V = 1871.45 \text{ \AA}^3$  (with estimated standard deviation in parenthesis). By interchanging the unit cell parameter  $a$  and  $c$ , the structure and structural parameters of BSTF (modified by Sr and Ti) can be correlated to the those of bismuth ferrite ( $\text{BiFeO}_3$ ).

The crystallite size ( $D$ ) of the specimen BSTF has been evaluated by using the broadening of the diffraction peaks, wavelength and Bragg angle in the standard Debye–Scherrer's formula;  $D = \frac{\lambda \times 0.89}{\cos \theta \times \beta}$ , here  $\theta$  = Bragg's angle,  $\beta$  = broadening of the peak of diffraction (which is evaluated at a half of the height of highest peak intensity in the radian and  $\lambda$  = the wavelength of  $\text{Cu K}\alpha$  ( $1.5406 \text{ \AA}$ ), [26]. The average crystallite size  $D$  of BSTF, calculated using many reselections, is found to be 52 nm.

The Goldschmidt tolerance factor ( $t$ ), which is one of the criterion for the predictability the formation of three dimension (3D) perovskite structure, is given by the equation as [5]:

$$t = \frac{r_A + r_X}{\sqrt{2}(r_B + r_O)} \quad (1)$$

where  $r_A$ ,  $r_B$ , and  $r_X$  are average ionic radii of A, B site cations and anion respectively. The calculated value of  $t$  for the studied compound BSTF is found to be 0.818. Most of the perovskites maintain 3D connectivity in the range of approximately  $0.813 \leq t \leq 1.107$ . The deviation from the ideal unit 1 clearly indicates the distortion of the crystal structure to rhombohedral symmetry.

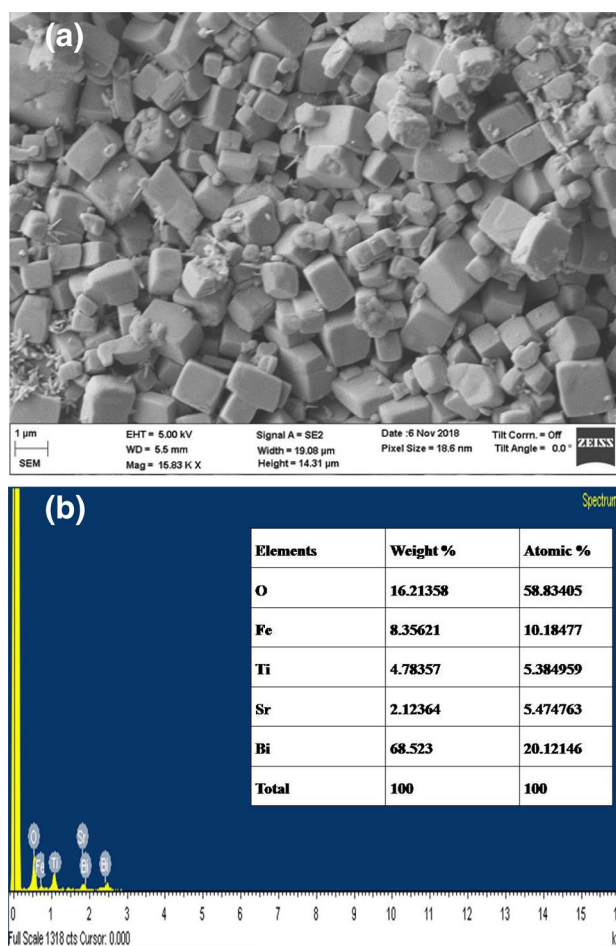


Fig. 2 **a** Scanning electron micrograph, **b** energy dispersive spectra of  $\text{Bi}(\text{Sr}_{0.25}\text{Ti}_{0.25}\text{Fe}_{0.5})\text{O}_3$

Another semiempirical geometrical parameter is  $\mu$ , which can be used to The Goldschmidt tolerance factor-predict the octahedral stability. The octahedral parameter  $\mu$  can be expressed as [5]:

$$\mu = \frac{r_B}{r_X} \quad (2)$$

Generally, the octahedra  $\text{BX}_6$  are stable in the range of 0.442 to 0.895. Here the octahedral parameter  $\mu$  is found to be 0.546. Thus, the calculated value of tolerance factor ( $t$ ) and octahedral parameter of our sample confirm the distortion in its cubic perovskite structure.

Figure 2a describes the scanning electron microscope of the BSTF pellet. It can be noticed that, the morphology of the sample consists of unlike shaped and sized grains, which are distributed uniformly throughout the surface with a few small voids. The energy dispersive spectrum (EDS) of the specimen is shown in Fig. 2b representing the compositional analysis. It suggests that the compound

contains Bi, Sr, Fe, Ti, O elements, and hence there is no source of other elements present in the sample. Detailed compositional analysis exhibits that the required amount of elements (with small deviation of 2–3%) is present in the prepared compound confirming the stoichiometry of the prepared compound. The weight % and atomic % and atoms per unit cell are given in Table (inset of Fig. 2b).

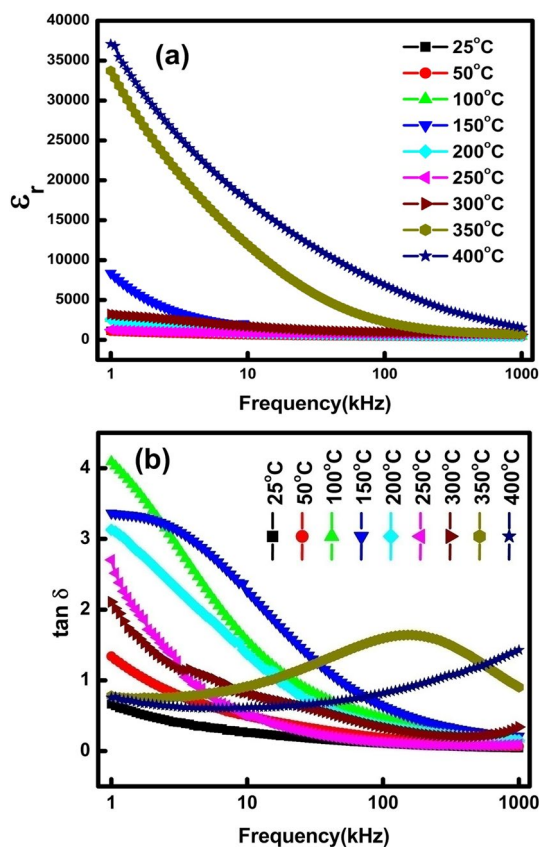
### 3.2 Studies of Dielectric Parameters

Figure 3a displays the frequency variation of  $\epsilon_r$  (relative permittivity) and loss factor ( $\tan \delta$ ) of the sample at various temperatures. The sample shows declining tendency of  $\epsilon_r$  and  $\tan \delta$  with rising in frequency, and assemble at unvarying value beyond definite frequency. From Fig. 3a, it can be observed that  $\epsilon_r$  diminishes incessantly with rising frequency. That kind of trend represents the dispersion owing to Maxwell–Wagner model [27]. The transfer of electron between  $\text{Fe}^{3+}$  and  $\text{Fe}^{2+}$  ions outcomes local displacement of charge carriers along the given electric field, which therefore, establishes polarization in ferrite sample. The reduction of  $\epsilon_r$  with respect to frequency is linked to the consequences of the hopping mechanism. In the region of

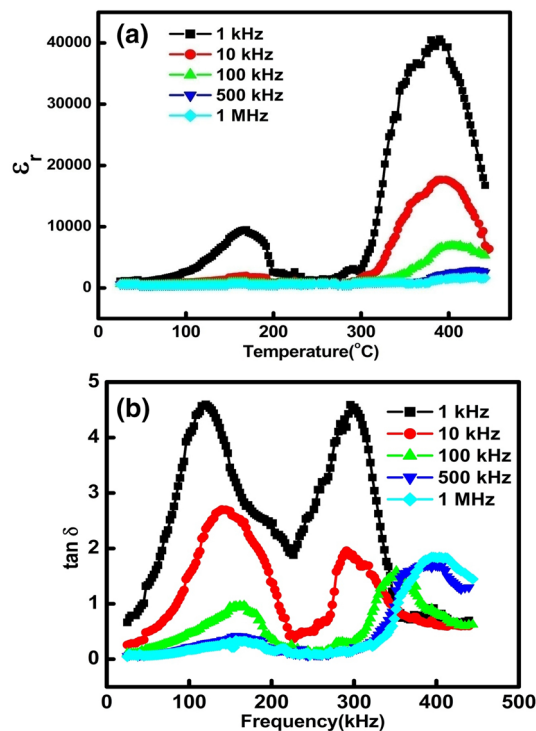
low-frequency, electrons, which are involved in the hopping between  $\text{Fe}^{3+} \rightarrow \text{Fe}^{2+}$  are aligned locally along the applied field direction, and describe the polarization process, and it results higher dielectric permittivity. But, as soon as the frequency of the electron hopping involving  $\text{Fe}^{3+} \rightarrow \text{Fe}^{2+}$  can't chase the fast-varying electric field, the polarization reduces with rising frequency and ultimately reaches an unvarying value. This is possible due to, with rising frequency; time taken by the given field switching its polarity eventually is smaller than the time responded by the electrons. For this reason, the applied field can't be responded by the electrons. The dipoles because of the inertia may not align themselves in the applied field direction at enough high frequencies, so  $\epsilon_r$  becomes almost constant [28, 29].

Figure 3b shows the dependence of loss factor along with frequency for BSTF sample and it decreases. In accordance with Koop's phenomenological model [27], the larger value of  $\tan \delta$  is described as the resistivity is higher, and then grain boundary effect is dominant in that region. So extra energy is required for the exchange of electrons for  $\text{Fe}^{3+} \rightarrow \text{Fe}^{2+}$  confined at grain boundary, so loss is higher. In high-frequency region, grains play a dominant role and resistivity is low. As less energy is required for hopping of the electrons, loss factor is less.

The temperature variation of dielectric constant at different frequency (1 kHz, 10 kHz, 100 kHz and 1000 kHz) is



**Fig. 3** a, b Variation of  $\epsilon_r$  and  $\tan \delta$  of  $\text{Bi}(\text{Sr}_{0.25}\text{Ti}_{0.25}\text{Fe}_{0.5})\text{O}_3$  with frequency at different temperatures



**Fig. 4** a, b Variation of  $\epsilon_r$  and  $\tan \delta$  of  $\text{Bi}(\text{Sr}_{0.25}\text{Ti}_{0.25}\text{Fe}_{0.5})\text{O}_3$  temperature at different frequency

illustrated in Fig. 4a. An extremely high dielectric constant peak is observed around 190 °C for BSTF system at room temperature. It is well known that bismuth ferrite experiences an antiferromagnetic transition at 370 °C and ferroelectric transition at 830 °C [30]. As this compound is a BiFeO<sub>3</sub> based compound, the temperature (190 °C) of the observed dielectric peak may be related to the much lower than the ferroelectric transition or Neel temperature of the BiFeO<sub>3</sub>. It is observed that there are two anomalies in the relative dielectric constant at 190 °C and at around 400 °C. The phase transition at 400 °C may be due to ferroelectric—paraelectric transition whereas similar to bismuth ferrite first anomaly may be related to magnetic transition.

Figure 4b shows the temperature dependence of loss factor for BSTF sample and it decreases. The increasing rate of tan δ is low in low temperature range and it increases rapidly at high temperature. A lot of charge carriers and defects are obtained across the sample leading to the conductivity rise. For this cause, at high temperature, there is a sharp increase in tan δ [31] (BSTF). In the plot, the shifting of peaks towards higher temperature on increasing the frequency suggest the relaxor type behavior.

### 3.3 Impedance Study

Complex impedance study is a well-known technique to inspect the electrical behavior of ceramics in respect of temperature and frequency. The impedance plot is used to expose the ionic contribution or additional defects in the sample. The contribution of bulk, grain boundary and electrode interfaces are disclosed by the correlation of microstructure and electrical responses [32–35].

The dielectric parameters of the sample (function of frequency) is normally illustrated by using  $Z^*$  (impedance),  $M^*$  (modulus) (dielectric constant), (loss tangent) which are related each other as follows:

$$Z^* = Z' - iZ'' = R_s - \frac{i}{\omega C_s}, \quad \epsilon^* = \epsilon' - i\epsilon''$$

$$M^* = M' + iM'' = i\omega C_0 Z^* \text{ and}$$

$$\tan \delta = \frac{\epsilon''}{\epsilon'} = \frac{-Z''}{Z'} = \frac{M''}{M'}$$

where  $\omega$  = angular frequency,  $C_s$  is capacitance and  $R_s$  are resistance, which are combined in series connection.

Figure 5a shows the variation of real part of impedance ( $Z'$ ) of BSTF with respect to frequency at different temperatures. It is to be noticed that the plots demonstrate dispersion at lower frequency merging at higher frequency, which create a stable range suggesting a release of space charge. The delay of relaxation process causes low frequency dispersion and it may be associated with space charges [36]. The

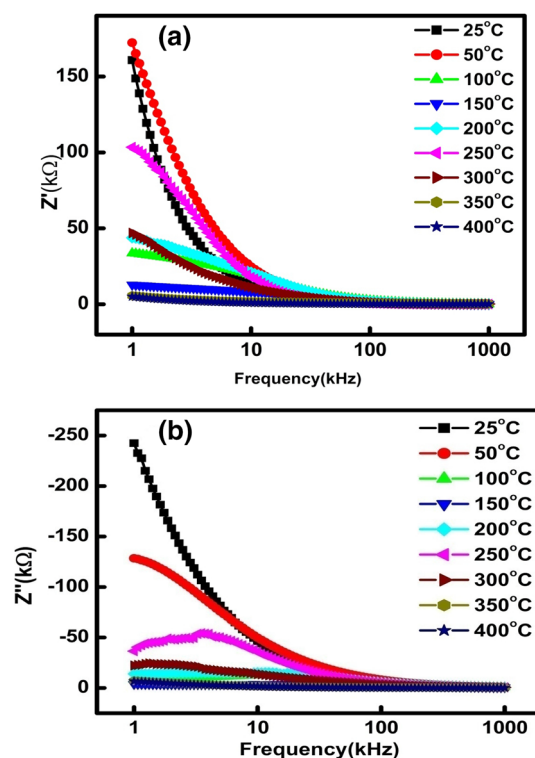


**Fig. 5** a, b Frequency dependence of  $Z'$  and  $Z''$  at some selected temperatures of Bi(Sr<sub>0.25</sub>Ti<sub>0.25</sub>Fe<sub>0.5</sub>)O<sub>3</sub>

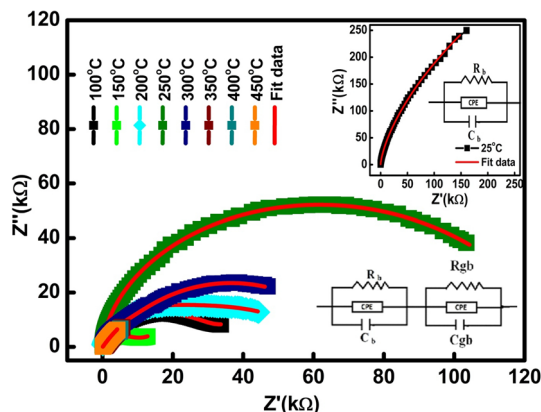
variation of  $Z'$  along with temperature is associated to both NTCR and PTCR like behaviour of the specimen.

Figure 5b represents the variation of imaginary component of impedance ( $Z''$ ) of BSTF along with frequency at diverse temperature. The  $Z''$  of the specimen has some essential features, for instance; (i) a reduction in  $Z''$  in the region of lower temperature, (ii) existence of peaks in  $Z''$  in the region of high temperature, and (iii) considerable enhancement in peak broadening along with the temperature. The absence of peaks in the  $Z''$  vs frequency plot for the BSTF compound illustrates the current dissipation lack in this range of temperature [37]. The occurrence of peaks at a specific frequency at higher temperature is called relaxation frequency ( $\omega_{\max}$ ), such that  $\omega_{\max}\tau = 1$ , (where  $\tau$  = relaxation time). The situation occurs due to the contribution of dipolar polarization. It may be noticed from the plots that,  $Z''_{\max}$  move to the high-frequency region, when the temperature rises suggesting the existence of temperature dependent dielectric relaxation process across the specimen. The relaxation process is because of the subsistence of the immobile/ electrons species at lower temperatures and vacancies/ defects at higher temperatures. Again, the peaks' broadening in respect of temperature commends the survival of the thermally activated relaxation process in the specimen. The change in peak width confirms a spread of relaxation time [38].

### 3.3.1 Nyquist Diagram

Figure 6 presents Nyquist plots of BSTF achieved at diverse temperatures in a wide frequency range (1 kHz–1 MHz). The Nyquist plots of the specimen can be analysed by the semi-circular arc plots whose model of succession changes along with the temperature. The annex of the semicircles' intercepts on the real impedance axis, and thus spectrum informs concerning electrical process occurring within the specimen. The relation between the spectrums and morphology of the compound is predicted by drawing a corresponding electrical circuit. The impedance behaviour of dielectrics consists of grains, grain boundaries and interfaces of sample/ electrode. The arc (semicircle) occurs at lower frequencies is due to the grain boundary and the interfaces. The arcs at high frequency suggest the bulk effect forming from the parallelly connected of grain capacitance ( $C_g$ ) and grain resistance ( $R_g$ ). Grains are semiconductor while the grain boundaries are insulating for polycrystalline sample. The semiconductor behavior in ceramic specimens is thought to be because of the oxygen loss at the sintering time [39].

It was mentioned above, the low frequency arcs portrays the grain boundary effect, while the semicircle at higher



**Fig. 6** Nyquist plot of  $\text{Bi}(\text{Sr}_{0.25}\text{Ti}_{0.25}\text{Fe}_{0.5})\text{O}_3$  at different temperatures

**Table 1** Comparison of the calculated values of bulk resistance ( $R_b$ ), grain boundary resistance ( $R_{gb}$ ), bulk capacitance ( $C_b$ ), grain boundary capacitance ( $C_{gb}$ ), at different temperatures

| Temperature (°C) | Model      | $R_g(\Omega)$ | $C_g$ (farad) | $R_{gb}(\Omega)$ | $C_{gb}$ (farad) |
|------------------|------------|---------------|---------------|------------------|------------------|
| 25               | (RQC)      | 2.158E+006    | 2.307E-010    | –                | –                |
| 50               | (RQC)      | 5.018E+005    | 1.511E-010    | –                | –                |
| 100              | (RQC)(RQC) | 3.592E+004    | 1.386E-010    | 1.113E+004       | 3.987E-008       |
| 150              | (RQC)(RQC) | 1.197E+004    | 3.365E-010    | 4.513E+004       | 2.855E-010       |
| 200              | (RQC)(RQC) | 5.279E+004    | 2.183E-010    | 1.220E+004       | 6.387E-010       |
| 250              | (RQC)(RQC) | 1.339E+005    | 2.749E-010    | 3.279E+001       | 2.069E-016       |
| 300              | (RQC)(RQC) | 2.775E+008    | 9.034E-010    | 6.082E+004       | 2.064E-017       |
| 350              | (RQC)(RQC) | 2.520E+010    | 2.723E-009    | 8.542E+002       | 1.739E-010       |
| 400              | (RQC)(RQC) | 3.086E+011    | 2.137E-022    | 4.612E+004       | 2.094E-009       |

frequency is considered as the bulk effect, and thus it can be obtained as the bulk capacitance ( $C_b$ ) and the bulk resistance ( $R_b$ ) which are connected in parallel. From the plot, at high temperatures, an apparent semicircular arc with a tendency to emerge another semicircle is observed. In these plots, the center of the arcs is noticed to be lower the real impedance axis. The semicircular arcs are obtained at high temperatures representing the electrical processes in the specimen, occurring due to the grains and grain boundaries contributions. The effect of blocking cores takes place because of generation of barrier potential from segregation of precipitates, and defect gathering at the grains' surface [40, 41]. By curve fitting, the measured quantity of the bulk resistance ( $R_g$ ), bulk capacitance ( $C_g$ ), grain boundary resistance ( $R_{gb}$ ), grain boundary capacitance ( $C_{gb}$ ) at various temperature are written in Table 1.

### 3.4 Electrical Modulus

It is a very significant tool used for analyzing and interpreting various dynamical aspects of transport (electrical) phenomenon, such as average relaxation time, conduction ions' hopping rate, etc. In the impedance spectra, the high resistance spectrum is dominating and the capacitance contribution can be determined using modulus spectroscopy [42].

In Fig. 7a, the change of the real part of  $M'$  along with frequency and temperature is shown. The  $M'$  value decreases with rise in temperature, and rises with increase in frequency showing a monotonous dispersion occurring due to the short range mobility of charge carriers and ions. This trend indicates that the grains are responsible for the electrical properties of the specimen. On the other hand, the trend of the charge flow to restore back is vanishing under induced electricfield. At high frequency, the  $M'$  value achieves maximum and at low frequency, the  $M''$  value achieves minimum ( $\sim 0$ ) suggesting the electrode polarization phenomena in the specimen [43, 44].

In Fig. 7b, variation of imaginary part ( $M''$ ) of modulus along with frequency and temperature is plotted. It can

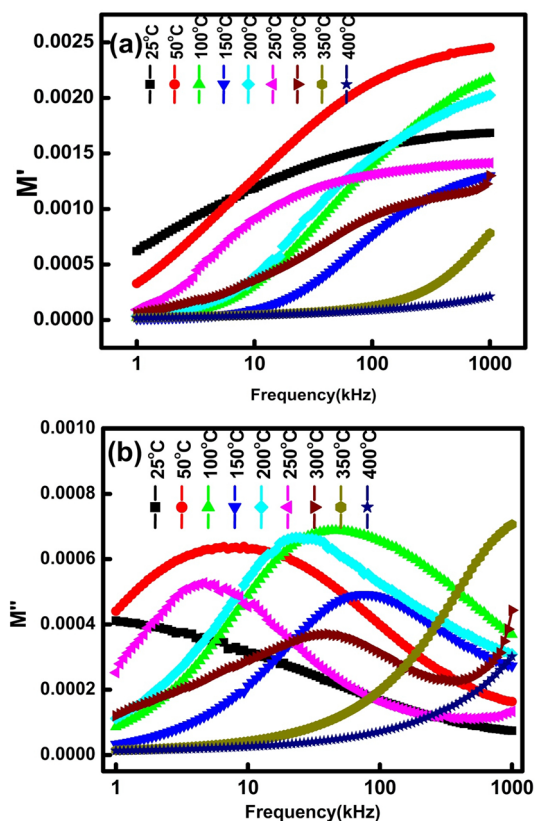


**Fig. 7** a, b Frequency dependence of  $M'$  and  $M''$  of  $\text{Bi}(\text{Sr}_{0.25}\text{Ti}_{0.25}\text{Fe}_{0.5})\text{O}_3$  at some selected temperature

be observed that as the temperature rises, the  $M''_{\text{max}}$  shifts towards high frequency. The frequency below the peak indicates the carriers are mobile in long ranges, whereas the frequency above the peak, the carriers are confined in a potential well and mobile in short range. So the  $f_{\text{max}}$  (where the peak occurs) suggests the transition from long range to short range of carriers in the specimen. The peaks are wider and asymmetry than the Debye curve [45, 46].

#### 4 Conductivity Studies

Figure 8a shows the changes of  $\sigma_{\text{ac}}$  (electrical conductivity) of BSTF in respect of frequency of the given electric field at different temperatures. The a.c. electrical conductivity can be calculated by utilizing the expression;  $\sigma_{\text{ac}} = 2\pi f \tan \delta \epsilon_r \epsilon_0$  where  $\tan \delta =$  tangent loss,  $f$  is the ac field frequency,  $\epsilon_0 =$  dielectric constant in vacuum [47]. The conductivity spectral arrangement suggests that the conductivity is frequency dependent for all temperatures.

Normally, the conductivity composes two components, the frequency independent part (dc conductivity) and the dispersive part (ac conductivity part). It can be clarified by Jonscher's power law.

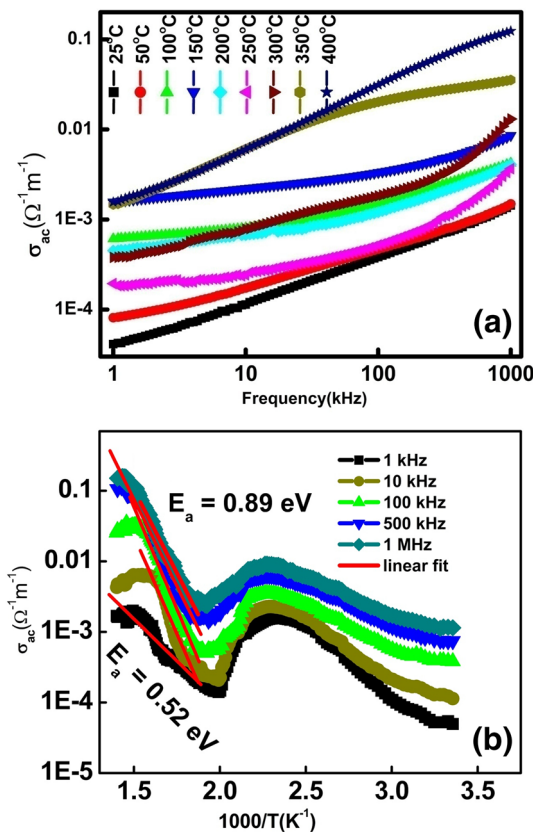


**Fig. 8** a, b Dependence of ac conductivity ( $\sigma_{\text{ac}}$ ) of  $\text{Bi}(\text{Sr}_{0.25}\text{Ti}_{0.25}\text{Fe}_{0.5})\text{O}_3$  at different temperature and frequency

$$\sigma_{\text{total}}(\omega) = \sigma_{\text{dc}} + A\omega^n = \sigma_{\text{dc}} + \sigma_{\text{ac}}$$

Here  $\sigma_{\text{ac}}(\omega) =$  ac conductivity,  $\sigma_{\text{dc}} =$  dc conductivity Here  $\omega = 2\pi f =$  angular frequency,  $n =$  temperature varying exponent and  $0 < n < 1$ .  $A =$  temperature varying factor and resolves the polarizability strength. Different like quantum tunneling, correlated barrier hopping model, small polaron hopping and overlapping large polaron tunneling are the various theoretical models, which can be explained by temperature varying exponent  $n$  [48, 49].

Here, in Fig. 8a, as the frequency independent dc conductivity part ( $\sigma_{\text{dc}}$ ) is absent, the conductivity part  $\sigma_{\text{ac}}(\omega)$  can be explained by the equation,

$$\sigma_{\text{ac}}(\omega) = A\omega^n$$

The exponent value ( $n$ ) is connected to numerous physical processes. The charge carriers' hopping may be associated with the translational motion for  $n$  is larger than 1 and for  $n$  is less than 1, it describes a confined small hopping of the carriers (charge). It recommends an major part of a thermal effect in this process (conduction) [41].

The slopes vary in dissimilar frequency ranges suggesting the survival of unlike conduction mechanisms. The conduction mechanism can be described by various theoretical models like correlated barrier hopping model, small polaron hopping, overlapping, Quantum mechanical tunneling and large polaron tunneling, etc. These models can describe temperature reliance of frequency exponent 'n' [48, 50, 51].

Figure 8b gives details about the changes of  $\sigma_{ac}$  (ac conductivity) in respect of temperature at different frequencies. The temperature rise leads to enhance  $\log \sigma_{ac}$ . It can be explained with reflecting on the hoping of charge carriers, which depends on temperature. This situation indicates the specimen's semiconductor nature. On the basis of the Arrhenius equation:  $\sigma_{dc} = \sigma_0 \exp(-E_a/k_B T)$ , where  $E_a$  = the charge carriers' activation energy,  $\sigma_0$  = pre-exponential factor and  $k_B$  = Boltzmann constant, we can evaluate  $E_a$  [52]. Utilizing this equation, the  $E_a$  values in different regions of temperature are mentioned in the corresponding places in all the graphs. The activation energy is supposed to contain contributions from the energies necessary for charge carriers creation and their free space movement. The defects in structure offer additional acceptor centers in the material at higher temperature [53].

#### 4.1 Polarisation Study

The polarization–electric field (P-E) loops of the sample BSTF (at different frequency) at room temperature are shown in Fig. 9. The existence of ferroelectricity in the specimen can be observed from the plot. In the specimen BSTF, ferroelectricity is produced due to the 6  $s^2$  orbital of Bi and 2p orbital of oxygen hybridisation. The manifestation of the P–E loop, which is unsaturated, is owing to the leakage current. It is to be noted that the specimen BSTF

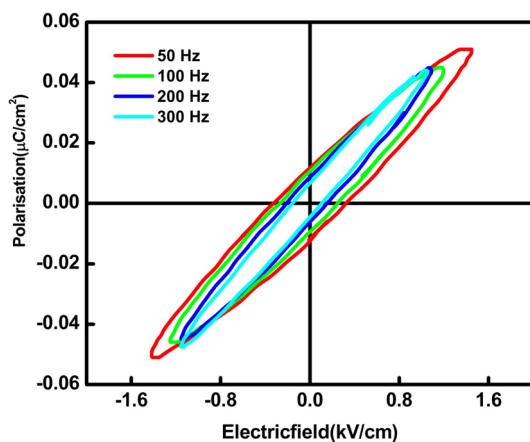
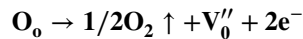


**Fig. 9** Frequency dependence of Polarisation loops of  $\text{Bi}(\text{Sr}_{0.25}\text{Ti}_{0.25}\text{Fe}_{0.5})\text{O}_3$  at room temperature

has been fabricated at higher temperature, which outcomes a small quantity of loss of oxygen and may be described as per the Kroger–Vink notation



where  $\text{O}_o$  is the loss of lattice oxygen.  $\text{V}_o''$  denotes oxygen vacancies.  $\text{e}^-$  is captured or released. These vacancies assist the leaky behavior of the compound. The remnant polarization ( $P_r$ ) is noted to be  $0.02 \mu\text{C}/\text{cm}^2$  at coercive field of 2 kV/cm for frequency 50 Hz.

As we decrease the frequency from 300 to 50 Hz keeping the applied electric field constant, the value of  $E_c$  and  $2P_r$  increases. The slight increase in the value of  $E_c$  and  $2P_r$  show that conduction process associated with frequency is slow.

#### 4.2 Leakage Current Study

Figure 10 presents the current density (J) versus electric field (E) plot at different temperature. It was observed that the current density is lower in the low-electric field region, which rises sharply with the rising electric field. The increase of leakage current with increase in electric field suggests that there can be certain conduction mechanism dominating in the conduction process. The leakage current mechanism was analyzed via the  $\log J$  versus  $\log E$ . It was found that the sample shows small-leakage current density ( $10^{-11} \text{ A}/\text{cm}^2$  at room temperature) suggesting that the compound is a good insulator. In Fig. 10, the slope is close to 1 indicating a probable Ohmic conduction.

### 5 Conclusion

In summary, perovskite type oxide BSTF was prepared by solid state route. We investigated that the single phase BSTF is a rhombohedral crystal system. The microstructure of

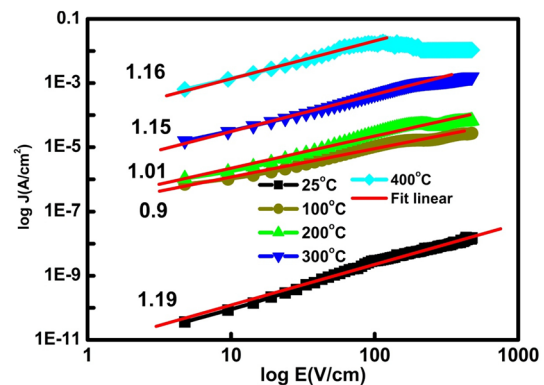


**Fig. 10** Variation of  $\log J$  with  $\log E$  at different temperature of  $\text{Bi}(\text{Sr}_{0.25}\text{Ti}_{0.25}\text{Fe}_{0.5})\text{O}_3$



the compound consists of grain and grain boundaries with small voids. Dielectric parameters of the specimen have been studied in the frequency region 1 kHz–1 MHz. The ferroelectricity in the specimen can be confirmed from the PE loop. Impedance study determined that occurrence of single semicircle arc at temperature  $\leq 50$  °C indicates the presence of bulk property and two arcs at temperature above 50 °C indicates both grain and grain boundary properties in the specimen. The non-Debye dielectric relaxation is seen in the specimen. As a better dielectric constant and low loss factor is detected in this compound at ambient temperature, it is appropriate for device application. The conductivity as a function of frequency suggests the thermally activated conduction process at various temperatures. From the study of leakage current characteristics, it was observed that the compound exhibits very low leakage current.

## References

1. T. Miyasaka, Lead halide perovskites in thin film photovoltaics: background and perspectives. *Bull. Chem. Soc. Jpn.* **91**, 1058 (2018)
2. K. Kamata, Perovskite oxide catalysts for liquid-phase organic reactions. *Bull. Chem. Soc. Jpn.* **92**, 133 (2019)
3. G. Rose, De perovskite, fossili novo, in *De novis quibusdam fossilibus quae in montibus uraliis inveniuntur*, ed. G. Rose (Schade, Schade, 1839)
4. A.K. Jena, A. Kulkarni, T. Miyasaka, Halide perovskite photovoltaics: background, status, and future prospects. *Chem. Rev.* **119**, 3036 (2019)
5. Y. Wei, Z. Cheng, J. Lin, An overview on enhancing the stability of lead halide perovskite quantum dots and their applications in phosphor-converted LEDs. *Chem. Soc. Rev.* **48**, 31 (2019)
6. A. Zeb, Y. Bai, T. Button, S.J. Milne, Temperature-stable relative permittivity from  $-70$  °C to  $500$  °C in  $(\text{Ba}_{0.8}\text{Ca}_{0.2})\text{TiO}_3\text{-Bi}(\text{Mg}_{0.5}\text{Ti}_{0.5})\text{O}_3\text{-NaNbO}_3$  ceramics. *J. Am. Ceram. Soc.* **97**, 2479 (2014)
7. R. Dittmer, E.M. Anton, W. Jo, H. Simons, J.E. Daniels, M. Hoffman, J. Pokorny, I.M. Reaney, J. Rödel, A high-temperature-capacitor dielectric based on  $\text{K}_{0.5}\text{Na}_{0.5}\text{NbO}_3\text{-modified Bi}_{1/2}\text{Na}_{1/2}\text{TiO}_3\text{-Bi}_{1/2}\text{K}_{1/2}\text{TiO}_3$ . *J. Am. Ceram. Soc.* **95**, 3519 (2012)
8. E. Cross, Lead-free at last. *Nature* **432**, 24 (2004)
9. Y. Saito, H. Takao, T. Tani, T. Nonoyama, K. Takatori, T. Homma, T. Nagaya, M. Nakamura, Lead-free piezoceramics. *Nature* **432**, 84 (2004)
10. T. Takenaka, H. Nagata, Y. Hirima, Y. Yoshii, K. Matumoto, C.Y. Fang, C.A. Randal, M.T. Lanagan, D.K. Agrawal, Microwave processing of electroceramic materials and devices. *J. Electroceram.* **22**, 125 (2009)
11. M.E. Lines, A.M. Glass, *Principles and Applications of Ferroelectric and Related Materials* (Clarendon, Oxford, 1977)
12. G.A. Somolenskii, I.E. Chupis, Ferroelectromagnets. *Sov. Phys. Usp.* **25**, 475–493 (1982)
13. X. Zhu, Q. Hang, Z. Xing, Y. Yang, J. Zhu, Z. Liu, Z. Zou, Microwave hydrothermal synthesis, structural characterization, and visible-light photocatalytic activities of single-crystalline bismuth ferric nanocrystals. *J. Am. Ceram. Soc.* **94**, 2688 (2011)
14. M.R. Biswal, J. Nanda, N.C. Mishra, S. Anwar, A. Mishra, Dielectric and impedance spectroscopic studies of multiferroic  $\text{BiFe}_{1-x}\text{Ni}_x\text{O}_3$ . *Adv. Mater. Lett.* **5**, 531 (2014)
15. L. Hongria, L. Zulib, L. Xiaolu, Y. Kailun, Effects of substitution of Ti for Fe in  $\text{BiFeO}_3$  films prepared by sol–gel process. *Phys B* **400**, 252 (2007)
16. Z.X. Cheng, A.H. Li, X.L. Wang, S.X. Dou, K. Ozawa, H. Kimura, S.J. Zhang, T.R. Shrout, Structure, ferroelectric properties, and magnetic properties of the La-doped bismuth ferrite. *J. Appl. Phys.* **103**, 07E507 (2008)
17. V.A. Khomchenko, V.V. Shvartsman, Crystal structure and magnetic properties of  $\text{Bi}_{0.8}(\text{Gd}_{1-x}\text{Ba}_x)_{0.2}\text{FeO}_3(x_{1/40}, 0.5, 1)$  multiferroics. *J. Phys. D* **42**, 045418 (2009)
18. V. Purohit, R.N.P. Choudhary, Fabrication and impedance spectroscopy of lead free magneto-electric compound:  $\text{Bi}(\text{Ca}_{0.25}\text{Ti}_{0.25}\text{Fe}_{0.5})\text{O}_3$ . *Appl. Phys. A* **125**, 125 (2019)
19. T. Kawae, H. Tsuda, A. Morimoto, Reduced leakage current and ferroelectric properties in Nd and Mn codoped  $\text{BiFeO}_3$  thin films. *Appl. Phys. Express* **1**, 051601 (2008)
20. J. Dhahri, M. Boudard, S. Zemni, H. Roussel, M. Oumezzine, Structure and magnetic properties of potassium doped bismuth ferrite. *J. Solid State Chem.* **181**(4), 802 (2008)
21. T. Hussain, S.A. Siddiqi, S. Atiq, M.S. Awanc, Induced modifications in the properties of Sr doped  $\text{BiFeO}_3$  multiferroics. *Prog. Nat. Sci. Mater. Int.* **23**, 487 (2013)
22. Y.P. Wang, L. Zhou, M.F. Zhang, X.Y. Chen, J.M. Liu, Z.G. Liu, Room-temperature saturated ferroelectric polarization in  $\text{BiFeO}_3$  ceramics synthesized by rapid liquid phase sintering. *Appl. Phys. Lett.* **84**, 1731 (2004)
23. A. Bismibanu, M. Alagar, J.S. Mercy-Jebaselvi, C. Gayathri, Preparation and characterization of bismuth ferrite nanoparticle using sol–gel method. *Int. J. Res. Appl. Sci. Eng. Technol.* **6**, 1767 (2018)
24. J. Wu, Z. Fan, J. Zhu, J. Wang, Multiferroic bismuth ferrite-based materials for multifunctional applications: ceramic bulks, thin films and nanostructures. *Prog. Mater. Sci.* **84**, 335 (2016)
25. E. Wu, *POWDMULT: An Interactive Powder Diffraction Data Interpretation and Indexing Program Version 2.1* (School of Physical Sciences, Flinders University of South Australia, Bradford Park, 1989)
26. V. Purohit, R. Padhee, R.N.P. Choudhary, Dielectric and impedance spectroscopy of  $\text{Bi}(\text{Ca}_{0.5}\text{Ti}_{0.5})_3$  ceramic. *Ceram. Int.* **44**, 3993–3999 (2017)
27. B.N. Parida, P.R. Das, Synthesis and characterization of a new ferroelectric oxide  $\text{Li}_2\text{Pb}_2\text{Pr}_2\text{W}_2\text{Ti}_4\text{Ta}_4\text{O}_{30}$ . *J. Alloys Compd.* **585**, 234 (2014)
28. D. Ravinder, Far-infrared spectral studies of mixed lithium–zinc ferrites. *Mater. Lett.* **40**, 205 (1999)
29. C.G. Koops, On the dispersion of resistivity and dielectric constant of some semiconductors at audio frequencies. *Phys. Rev.* **83**, 121 (1951)
30. P. Uniyal, K.L. Yadav, Pr doped bismuth ferrite ceramics with enhanced multiferroic properties. *J. Phys. Condens. Matter.* **21**, 405901 (2009)
31. V. Purohit, R.N.P. Choudhary, Structural, dielectric and impedance properties of lead-free  $\text{Bi}(\text{Sr}_{0.5}\text{Ti}_{0.5})\text{O}_3$  ceramic. *Mater. Sci. Eng. B* **243**, 30–37 (2019)
32. S. Brahma, R.N.P. Choudhary, A.K. Thakur, AC impedance analysis of  $\text{LaLiMo}_2\text{O}_8$  electroceramics. *Phys B* **355**, 188 (2005)
33. J.R. Macdonald, *Impedance Spectroscopy: Emphasizing Solid Materials and Systems, Chap. 4* (Wiley, New York, 1978)
34. J. Suchanicz, The low-frequency dielectric relaxation  $\text{Na}_{0.5}\text{Bi}_{0.5}\text{TiO}_3$  ceramics. *Mater. Sci. Eng. B* **55**, 114 (1998)
35. T. Acharya, R.N.P. Choudhary, Structural, dielectric and impedance characteristics of  $\text{CoTiO}_3$ . *Mater. Chem. Phys.* **17**, 131 (2016)

36. V. Purohit, R. Padhee, R.N.P. Choudhary, Structural and electrical properties of Bi(Mg<sub>0.5</sub>Ti<sub>0.5</sub>)O<sub>3</sub> ceramic. *J. Mater. Sci. Mater. Electron.* **29**, 5224 (2018)
37. A. Shukla, N. Kumar, C. Behera, R.N. Choudhary, Structural, dielectric and magnetic characteristics of Bi(Ni<sub>0.25</sub>Ti<sub>0.25</sub>Fe<sub>0.50</sub>)O<sub>3</sub> ceramics. *J. Mater. Sci. Mater. Electron.* **27**, 1209–1216 (2016)
38. S. Nath, S.K. Barick, S. Hajra, R.N.P. Choudhary, Studies of structural, impedance spectroscopy and magnetoelectric properties of (SmLi)<sub>1/2</sub>(Fe<sub>2/3</sub>Mo<sub>1/3</sub>)O<sub>3</sub> electroceramics. *J. Mater. Sci. Mater. Electron.* **29**, 12251 (2018)
39. D.K. Mahato, A. Dutta, T.P. Sinha, Impedance spectroscopy analysis of double perovskite Ho<sub>2</sub>NiTiO<sub>6</sub>. *J. Mater. Sci.* **45**, 6757 (2010)
40. S. Mahajan, O.P. Thakur, D.K. Bhattacharya, K. Sreenivas, Ferroelectric relaxor behaviour and impedance spectroscopy of Bi<sub>2</sub>O<sub>3</sub>-doped barium zirconium titanate ceramics. *J. Phys. D* **42**, 065413 (2009)
41. J.H. Park, J.S. Bae, B.C. Choi, J.H. Jeong, Impedance spectroscopy of Bi<sub>3.25</sub>La<sub>0.75</sub>Ti<sub>3</sub>O<sub>12</sub> ceramics above and below ferroelectric transition temperatures. *J. Phys. D* **40**, 579 (2007)
42. R. Gerhardt, Impedance and dielectric spectroscopy revisited: distinguishing localized relaxation from long-range conductivity. *J. Phys. Chem. Solids* **55**, 1491–1506 (1994)
43. R. Rai, I. Coondoo, R. Rani, I. Bdikin, S. Sharma, A.L. Kholkin, Impedance spectroscopy and piezoresponse force microscopy analysis of lead-free (1-x) K<sub>0.5</sub>Na<sub>0.5</sub>NbO<sub>3</sub>-xLiNbO<sub>3</sub> ceramics. *Curr. Appl. Phys.* **13**, 430 (2013)
44. M.K. Shamim, S. Sharma, S. Sinha, E. Nasreen, Dielectric relaxation and modulus spectroscopy analysis of (Na<sub>0.47</sub>K<sub>0.47</sub>Li<sub>0.06</sub>)NbO<sub>3</sub> ceramics. *J. Adv. Dielectr.* **7**, 1750020 (2017)
45. S. Thakur, R.H. Rai, I. Bdikin, M.A. Valentec, Impedance and modulus spectroscopy characterization of Tb modified Bi<sub>0.8</sub>A<sub>0.1</sub>Pb<sub>0.1</sub>Fe<sub>0.9</sub>Ti<sub>0.1</sub>O<sub>3</sub> ceramics. *Mater. Res.* **19**, 1–8 (2016)
46. S. Pattanayak, B. Parida, P.R. Das, R. Choudhary, Impedance spectroscopy of Gd-doped BiFeO<sub>3</sub> multiferroics. *Appl. Phys. A* **112**, 387–395 (2013)
47. S. Halder, K. Parida, S.N. Das, S.K. Pradhan, S. Bhuyan, R.N.P. Choudhary, Dielectric and impedance properties of Bi(Zn<sub>2/3</sub>V<sub>1/3</sub>)O<sub>3</sub> electronic material. *Phys. Lett. A* **382**, 716 (2016)
48. M. Pollak, T.H. Geballe, Low-frequency conductivity due to hopping processes in silicon. *Phys. Rev.* **122**, 1742 (1961)
49. E. Veena-Gopalan, K.A. Malini, S. Sagar, D. Sakthi-Kumar, Y. Yoshida, I.A. Al-Omari, M.R. Anantharaman, Mechanism of ac conduction in nano-structured manganese zinc mixed ferrites. *J. Phys. D* **42**, 165005 (2009)
50. F.A. Abdel-wahab, H.M. Maksoud, M.F. Kotkata, Electrical conduction and dielectric relaxation in semiconductor SeSm<sub>0.005</sub>. *J. Phys. D* **39**, 190 (2006)
51. A. Ghosh, S. Bhattacharya, D.P. Bhattacharya, A. Ghosh, Frequency dependent conductivity of cadmium vanadate glassy semiconductor. *J. Phys. Condens. Matter* **20**, 035203 (2008)
52. K. Parida, S.K. Dehury, R.N.P. Choudhary, Structural, electrical and magneto-electric characteristics of BiMgFeCeO<sub>6</sub> ceramics. *Phys. Lett. A* **380**, 4083 (2016)
53. M. Ram, Electrical characteristics of Li(Ni<sub>7/10</sub>Fe<sub>3/10</sub>)VO<sub>4</sub> ceramics. *J. Alloys Compd.* **509**, 1744 (2011)

**Publisher's Note** Springer Nature remains neutral with regard to jurisdictional claims in published maps and institutional affiliations.